# Voronoi Based Coverage Control with Anisotropic Sensors and Experimental Case Study

**Abstract** In this paper we investigate coverage control problem for mobile sensor networks. The novelty is to consider an anisotropic sensor model whose performance depends not only on the distance but also on the orientation to a target point. By adapting Lloyd algorithm, a distributed control law is derived. Aside from coverage, we also show that the control law guarantees collision avoidance between the agents. The performance of the control laws is demonstrated through not only numerical simulation but also experiments on a mobile robot test bed.

**Keywords** Anisotropic sensors · Voronoi tessellations · Lloyd algorithm · Distributed algorithms

## 1 Introduction

Stimulated by technological advances and development of relatively inexpensive communication, computation, and sensing devices, the interest in the research area of cooperative control of multi-agent systems has majorly increased over the last decades. In multi-agent systems, each individual is assumed to have abilities to sense its immediate environment, communicate with others, process information gathered and take a local action based on the information gathered. Key aspects of designing the control laws for motion coordination are that each agent has to behave without any leader (leader-less) and based on its local information (i.e. the control law is distributed) due to limited communication and sensing capabilities. This is also inspired by the behaviour of biological systems such as school of fish, flocking of birds and animal herds that exist in nature.

In this paper our focus is on deployment of a mobile sensing network of vehicles equipped with sensors to sample the environment. Such problem is called a coverage control

Address(es) of author(s) should be given

problem. Coverage control has a closed relation with sensor networks. A sensor network consists of a collection of sensing devices that can coordinate their actions through wireless communication and aim at performing tasks such as collecting data over a region of interest. Sensor networks usually consist of stationary sensor nodes. The deployment of a static network is often either human monitored or random, depending on the environment. It can be predetermined when the environment is sufficiently known, in which case, sensors can be strategically hand placed e.g. the art gallery problem where the goal is to determine position and minimal number of cameras in a building or gallery so that every point in the building is observed by at least one camera. However, if the environment is unknown, hostile or even dangerous for humans, the deployment cannot be determined *a priori* in which case sensors may be air-dropped from an aircraft, generally resulting in a random configuration. Sometimes, deploying such a stationary sensor network and maintaining its sensing coverage could be a difficult task. For example, imagine deploying a stationary sensor network over a region of interest. Even though advanced tools like airplanes are available to make the deployment safer and easier, various factors such as winds and obstacles are very likely to introduce coverage holes regardless of how many sensor nodes are dropped. Even if a perfect coverage can be achieved initially, events such as sensor failures will certainly degrade coverage performance as time evolves.

Due to the problem of stationary sensor networks, there is an urgent need for sensor nodes to be equipped with mobility for instance by installing sensors on autonomous vehicles or robots. Mobility brings some improvements to the performance of sensor networks. First, the sensor nodes are able to autonomously re-deploy themselves that maximizes the coverage of the environment. Second, by adapting their configuration, the network will remain robust to environment changes due to sensors departures, arrivals or mal-

function and also communication links' failures. Moreover, mobile sensors can undertake challenging tasks that can be too dangerous for human intervention such as search and recovery operations, manipulation in hazardous environments, surveillance, wild fire detection and also environmental monitoring for pollution detection and estimation .

Some relevant works on coverage control problem are [1–10]. In [1] the agents move to an optimal configuration which minimizes an objective function. The approach is based on Voronoi tessellation and Lloyd algorithm. Briefly speaking, the agents partition a given region into subregions given by Voronoi partitions and move towards the centroid of its subregion, which increases its sensing radius until the whole area is covered. The same problem is considered in [2] with a more realistic model by introducing "limited-range interactions" of the sensors, i.e the sensing range is restricted to a bounded region. Power-aware coverage algorithms for mobile networks are proposed in [3] in order to balance the energy expenditure accross the network and make nodes with high power compensate for nodes with low power. The advantage of Voronoi approach is that the control law is distributed by its nature. Alternative approaches are introduced in [4–6]. In [4] the authors consider a probabilistic network model and a density function to represent the frequency of random events taking place over the mission space. The authors develop an optimization problem that aims at maximizing coverage using sensors with limited ranges, while minimizing communication cost. A potential-field-based approach to deployment problem in an unknown environment is presented in [5]. Reference [6] proposed an inverse agreement control strategy that forces the agents to disperse in a workspace. Here each agent follows a flow, whose inverse would lead the team to an agreement.

Moreover, the reference [7] considers dynamic coverage. Here, the agents move so that every point in a given area is sensed with a pre-specified coverage level $C^*$. Authors in [8] present a coverage control algorithm taking account of information decay w.r.t time. Dynamic coverage under some practical assumptions such as bounded sensing and actuation capacities of the vehicles are addressed in [9, 10]. However, in the works mentioned above, only a uniform (isotropic) sensor model is considered.

In this paper, in contrast to the above papers, we consider coverage problem with an anisotropic sensor model. This model is more realistic since most of sensors such as cameras, directional microphones, radars etc are anisotropic. In this paper, one of the main objectives is to investigate the applicability of Voronoi based approach in [1] to tackle coverage problem with anisotropic sensors. For this reason, as a first approach we assume a specific class of anisotropic sensors with elliptic sensing performance level sets as one way of achieving a possibly better approximation to sensor characteristics instead of circles as for the isotropic case. One example of sensors that satisfy this model is radar [11]. Moreover, the study of coverage control problem via experiments performed on a mobile robotic platform is another goal of this paper.

Consideration of a general anisotropic sensor model results in an anisotropic Voronoi tesselation which leads to non-distributed control law, as we will discuss later. However, by assuming fixed and equal sensor orientations, the control law is shown to be distributed. The idea of deriving a control law for the considered anisotropic sensor model is to transform an anisotropic problem to the isotropic one. By the transformation properties, the control law obtained for the isotropic problem also solves the problem in the anisotropic case.

This paper is organized as follows: The problem formulation for anisotropic sensor model is presented in Section 2. Anisotropic Voronoi partition which is an extension of the ordinary Voronoi partition in Lloyd algorithms and the optimal location of mobile sensors are derived in Section 3. In Section 4 the control law for a deployment is derived and collision avoidance is investigated. We validate our results through simulations and experiments in Section 5 and 6 respectively. Finally, in Section 7 we draw some conclusions and provide future directions of research.

## 2 Problem formulation

Let $Q$ be a convex polytope in $\mathbb{R}^2$ including its interior. $\phi(\cdot) : Q \to \mathbb{R}_+$ is a continuous distribution density function which may represent a probability that some event takes place in $Q$ or relative important of each point in $Q$. Let $P = (p_1, ..., p_n)$ be the location of $n$ identical mobile sensors moving in $Q$. Let $\Theta = (\theta_1, ..., \theta_n)$ be the orientation/attitude of $n$ sensors. It is assumed that each sensor could get information about its own location and orientation (e.g. by using GPS technology, compass). Moreover, each sensor is equipped with omni-directional communication capability so that it could send information to others i.e. allowing cooperation between the sensors. Another assumption that is considered for the analysis is either the sensors have a sufficient sensing range or the number of sensors are sufficient such that the region of interest $Q$ can be covered by them. This assumption is necessary to avoid the existance of coverage hole. The non-decreasing differentiable function $f(\cdot) :$ $\mathbb{R}_+ \to \mathbb{R}_+$ indicates the sensing performance of a sensor, i.e the probability of sensing an event in $Q$. Reference [1] considered an isotropic sensor with a sensing performance defined as $f(\|q - p_i\|)$ that degrades with the distance between a point $q \in Q$ and the $i$-th sensor position $p_i$. Points where sensing performance (or probability of sensing) is equal are represented by a circle of radius $R$ centered at the sensor location. As shown in Figure 1(a), points $q_1$ and $q_2$ with the
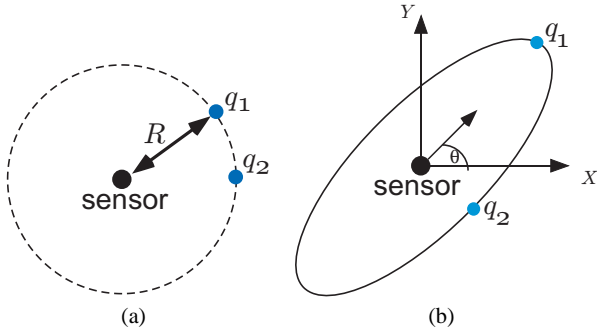
**Fig. 1** (a) Isotropic sensor model, (b) Anisotropic sensor model

same distance to the sensor will result in a same sensing probability.

In this paper, anisotropic sensors are considered where the degradation of sensing performance is also affected by the orientation of the sensor w.r.t a point to be sensed. The anisotropic sensor model in this paper is considered by a non-Euclidean distance measure as follows.

**Assumption 1** *The sensing performance of anisotropic sensor model is given by the non-Euclidean distance measure $\|q - p_i\|_{\mathbf{L_i}}$ defined as*

$$\|q - p_i\|_{\mathbf{L_i}}^2 = (q - p_i)^T \mathbf{L}_i (q - p_i), \tag{1}$$

*where matrix $\mathbf{L_i}$ is positive definite and can be decomposed as $\mathbf{L_i} = \mathbf{F_i^T F_i}$ with*

$$\mathbf{F_i} = \begin{pmatrix} \frac{c}{a} & 0 \\ 0 & \frac{c}{b} \end{pmatrix} \begin{pmatrix} \cos\theta_i & \sin\theta_i \\ -\sin\theta_i & \cos\theta_i \end{pmatrix} \tag{2}$$

*where $\theta_i$ is the orientation of i-th sensor, and $a,b,c > 0$ are scalar parameters which are determined by sensors' characteristics.*

Observe that matrix $\mathbf{F_i}$ is invertible. The level sets of the sensing performance of the anisotropic sensor are given by ellipses centered at the sensor location as shown in Figure 1(b). Here, $\theta_i$ is the orientation of an ellipse, $a,b$ represent the length of major and minor axis of an ellipse respectively. $c$ is a scale factor that decides the sensing performance on a certain level set.

The overall sensing cost incurred by all sensors can be formulated as

$$\mathcal{H}(P,\Theta,\mathcal{W}) = \sum_{i=1}^{n} \int_{W_i} f(\|q - p_i\|_{\mathbf{L_i}})\phi(q)dq, \tag{3}$$

where region $W_i$ is the dominance region of the $i$-th sensor and $\mathcal{W} = (W_1,...,W_n)$. The challenges addressed in this paper are

1. Find the optimal configuration such that

$$\min_{P,\Theta,\mathcal{W}} \mathcal{H}. \tag{4}$$

2. Find the control law $u_i$ that drives mobile sensors to the optimal configuration given mobile sensors dynamics

$$\dot{p}_i = u_i. \tag{5}$$

Optimal coverage is achieved by minimizing (3) w.r.t (1) sensor location $P$ and orientation $\Theta$ and (2) the assignment of dominance regions $\mathcal{W}$.

## 3 Optimal partition and location

### 3.1 Anisotropic Voronoi partitions

To minimize (3), we introduce the notion of Voronoi partition. The Voronoi region of a sensor is defined by all points which are "closer" in the sense of the considered distance measure to that sensor than to any other. For the Euclidean distance measure, Voronoi region $V_i$ associated with its generator $p_i$ is defined as

$$V_i = \{q \in Q | \|q - p_i\| \leq \|q - p_j\|, \forall j \neq i\}. \tag{6}$$

Voronoi partition for the anisotropic case considered in this paper is defined as follows.

**Definition 1** For the non-Euclidean distance measure (1), the anisotropic Voronoi tessellation $V_i^*$ associated with its generator $p_i$ is

$$V_i^* = \{q \in Q | \|q - p_i\|_{\mathbf{L_i}} \leq \|q - p_j\|_{\mathbf{L_j}}, \forall j \neq i\}. \tag{7}$$

This anisotropic Voronoi partition is not only determined by the sensors position but also the sensors orientation $\theta_i$ as observable from matrix $\mathbf{L_i}$. As a result the anisotropic Voronoi tesselation is no longer composed of convex polytopes, but of curved possibly non-convex regions. Figures 2(a) and 2(b) depict the examples of isotropic and anisotropic Voronoi partition respectively.

**Lemma 1** *The boundary between two adjacent $V_i^*$ and $V_j^*$ as defined in (7) is a quadratic curve.*

*Proof* Any point $q$ in $V_i^* \cap V_j^*$ which is the boundary of Voronoi partitions $V_i^*$ and $V_j^*$ satisfies $\|q - p_i\|_{\mathbf{L_i}} = \|q - p_j\|_{\mathbf{L_j}}$ i.e. $(q - p_i)^T \mathbf{L}_i(q - p_i) = (q - p_j)^T \mathbf{L}_j(q - p_j)$. It is clear that this equation is quadratic in $q$. Therefore any point in $V_i^* \cap V_j^*$ lies on a quadratic curve.

The boundary can be represented as

$$\begin{bmatrix} x \\ y \\ 1 \end{bmatrix}^T \begin{bmatrix} A & \frac{1}{2}C & \frac{1}{2}D \\ \frac{1}{2}C & B & \frac{1}{2}E \\ \frac{1}{2}D & \frac{1}{2}E & K \end{bmatrix} \begin{bmatrix} x \\ y \\ 1 \end{bmatrix} = 0, \tag{8}$$

where $A,B,C,D,E,K$ in (8) can be computed by solving $(q-p_i)^T\mathbf{L}_i(q-p_i) = (q-p_j)^T\mathbf{L}_j(q-p_j)$. Due to the space limitation, only $A,B,C$ are described which will be used later in this paper. The coefficients of (8) are : $q = (x,y)$, $A =$
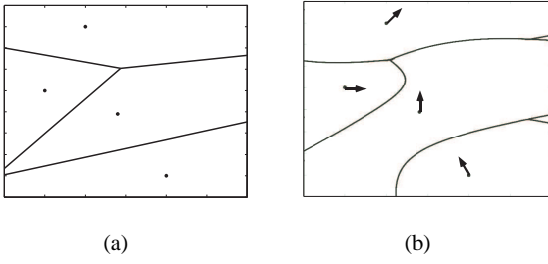
**Fig. 2** (a) Isotropic Voronoi partition, (b) Anisotropic Voronoi partition given by (7). As can be seen, the regions on the right side have no generators inside.
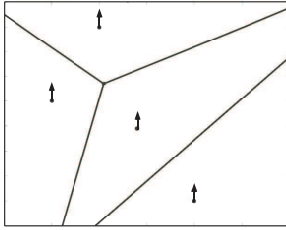


**Fig. 3** Anisotropic Voronoi partition with equal orientation

$b^2(\cos^2\theta_i - \cos^2\theta_j) + a^2(\sin^2\theta_i - \sin^2\theta_j)$, $B = a^2(\cos^2\theta_i - \cos^2\theta_j) + b^2(\sin^2\theta_i - \sin^2\theta_j)$, $C = (a^2 - b^2)(\sin 2\theta_i - \sin 2\theta_j)$ and $D, E \neq 0$.

Another major difference to isotropic Voronoi tesselations is that anistropic tesselations may contain regions without a generator [12], i.e. a Voronoi cell of an anisotropic Voronoi diagram is not necessarily connected. Moreover, the information of all other sensor positions is required to compute anisotropic Voronoi diagrams. The complexity of a 2-dimensional $n$ number of agents anisotropic Voronoi partition is in $O(n^{2+\varepsilon})$, where $\varepsilon$ is an arbitrary (small) positive constant ( [12]).

*Remark 1* By using a gradient flow approach, the sensors converge to a set of critical points. However, since the information of all sensor positions is necessary to construct anisotropic Voronoi diagrams, the resulting control law will be non-distributed. This is in contrast to isotropic Voronoi diagram where only Delaunay neighbor (agents which have adjacent Voronoi cells) positions are required.

As mentioned above, in general i.e. for the arbitary orientation of the sensors, the Voronoi approach results in a non-distributed control law. Therefore, for the remainder of this paper, a more specific case given by the following assumption is considered.

**Assumption 2** *The orientations of all sensors are equal and fixed over time, i.e. $\theta_i(t) = \theta_j(t) = \theta, \forall i \neq j$ and $t \geq 0$.*

This can be achieved by applying a known method (e.g [13]) for making an agreement on the orientation beforehand.

This assumption leads to the following lemma.

**Lemma 2** *From assumption 2 and definition 1, anisotropic Voronoi tessellation is composed of convex polytopes. Moreover, $\mathbf{F_i}(\mathbf{t}) = \mathbf{F_j}(\mathbf{t}) = \mathbf{F}$ and $\mathbf{L_i}(\mathbf{t}) = \mathbf{L_j}(\mathbf{t}) = \mathbf{L}$, $\forall i \neq j$ and $t \geq 0$.*

*Proof* From assumption 2, $\theta_i = \theta_j = \theta$, it follows that $A = B = C = 0$ in (11) and furthermore $D, E \neq 0$. As a result, the boundary of the Voronoi cell is a straight line. Since $Q$ is a convex polytope, the Voronoi tessellation is also composed of convex polytopes. From (2), it is also cleared that $\mathbf{F_i} = \mathbf{F}$ and $\mathbf{L_i} = \mathbf{L}$.

One example of anisotropic Voronoi diagram with fixed and equal orientations is shown in Figure 3.

### 3.2 Local optimal location

In this subsection, positions of mobile sensors that (locally) minimize (3) is derived. First (3) is minimized w.r.t. sensor's partition i.e. we would like to find out what kind of partition (dominance region) is necessary to minimize (3) for given sensors' location (sensors' location are fixed).

**Lemma 3** *Anisotropic Voronoi partition $\mathcal{V}^*$ minimizes (3) w.r.t partition $\mathcal{W}$.*

*Proof* From definition 1 and since $f$ is a non-decreasing function, it is clear that Voronoi partition $\mathcal{V}^*$ minimizes (3) w.r.t partition $\mathcal{W}$.

As the orientation is assumed to be fixed and as a result of lemma 3,

$$\min_{P,\Theta,\mathcal{W}} \mathcal{H} = \min_P \mathcal{H}_{\mathcal{V}^*}. \tag{9}$$

Assume that the sensing performance $f(\|q - p_i\|_{\mathbf{L}}) = \|q - p_i\|_{\mathbf{L}}^2$. Then (3) can be written as

$$\mathcal{H}_{\mathcal{V}^*}(P) = \sum_{i=1}^n \int_{V_i^*} \|q - p_i\|_{\mathbf{L}^2} \phi(q) dq. \tag{10}$$

In order to derive the optimal location of sensors, the above equation can be simplified to

$$\mathcal{H}_{\mathcal{V}^*}(P) = \sum_{i=1}^n \int_{V_i^*} \|\mathbf{F}(q - p_i)\|^2 \phi(q) dq. \tag{11}$$

Next, we introduce anisotropic centroidal Voronoi configuration.

**Definition 2** Given the set of points $P$ in $Q$. $C_{V_i^*}$ is the center of mass (centroid) of an anisotropic Voronoi partition. A Voronoi tessellation is called an anisotropic centroidal Voronoi configuration if

$$p_i = C_{V_i^*}, \forall i; \tag{12}$$

i.e the points $P$ serve as generators and also centroids in terms of anisotropic Voronoi tessellations.

The optimal location is given by the following proposition.

**Proposition 1** *The objective function (11) is minimized by the anisotropic centroidal Voronoi configuration.*

*Proof* Define $\bar{q}, z_i$ as $\bar{q} = \mathbf{F}q$ and $z_i = \mathbf{F}p_i$ which are points of region and sensors in a space transformed by matrix $F$ called a solution space. Note that the region $Q$ is transformed by $\mathbf{F}$ to a convex region $Q_s$ and minimization of (11) in the solution space leads to minimization in the real physical space. Moreover, from (7) and by applying transformation matrix $\mathbf{F}$, the anisotropic Voronoi partition $V_i^*$ is transformed to isotropic Voronoi partition $(\bar{V}_i)$ in the solution space defined as

$$\bar{V}_i = \{\bar{q} \in Q_s | \|\bar{q} - z_i\| \le \|\bar{q} - z_j\|, \forall j \ne i\}. \tag{13}$$

By applying substitution rule for multiple variables, the integral in (11) can be rewritten as :

$$\mathscr{H}_{\mathscr{Z}}(Z) = \sum_{i=1}^{n} \int_{\bar{V}_i} \|\bar{q} - z_i\|^2 \phi(\bar{q}) \left| \det(\mathbf{F}^{-1}) \right| d\bar{q}. \tag{14}$$

with $\mathscr{Z} = (z_1, ..., z_n)$. Applying the parallel axis theorem, (14) becomes

$$\mathscr{H}_{\bar{V}}(Z) = \left| \det(\mathbf{F}^{-1}) \right| \left( \sum_{i=1}^{n} J_{\bar{V}_i, C_{\bar{V}_i}} + \sum_{i=1}^{n} M_{\bar{V}_i} \|z_i - C_{\bar{V}_i}\|^2 \right), \tag{15}$$

where

$$M_{\bar{V}} = \int_{\bar{V}} \phi(\bar{q}) d\bar{q}, \quad C_{\bar{V}} = M_{\bar{V}}^{-1} \int_{\bar{V}} \bar{q} \phi(\bar{q}) d\bar{q}, \tag{16}$$

$$J_{\bar{V}, z} = \int_{\bar{V}} \|\bar{q} - z\|^2 \phi(\bar{q}) d\bar{q}. \tag{17}$$

denote mass, centroid and polar moment of inertia of an anisotropic Voronoi partition respectively. The local minimum is the solution of

$$\nabla \mathscr{H}_{\mathscr{Z}} = [... \frac{\partial \mathscr{H}_{\bar{V}}}{\partial z_i} ...]^T = \mathbf{0}, \tag{18}$$

with the partial derivative of (14) given by

$$\frac{\partial \mathscr{H}_{\bar{V}}}{\partial z_i}(Z) = 2 \left| \det(\mathbf{F}^{-1}) \right| M_{\bar{V}_i}(z_i - C_{\bar{V}_i}). \tag{19}$$

The local minimum points given by $z_i = C_{\bar{V}_i}$ i.e. critical points for $\mathscr{H}_{\bar{V}}$ are centroids of the Voronoi cells in the solution space which are centroids $C_{V_i^*} = \mathbf{F}^{-1} C_{\bar{V}_i}$ of the anisotropic Voronoi partitions.

## 4 Continuous Lloyd descent for coverage control

### 4.1 Optimal control for fixed orientation

In this section, a control law based on Lloyd algorithm to drive sensors to the location that minimizes (3) is derived.
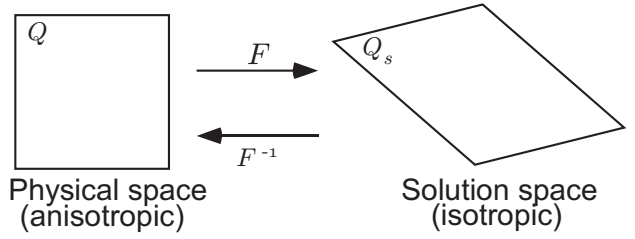


**Fig. 4** Transformation between solution and real space

The strategy is to transform the control law in the solution space into the real physical space as illustrated in Figure 4.

Consider sensors in real space with dynamics given in (5). Set

$$u_i = -k(p_i - C_{V_i^*}), \tag{20}$$

where $k$ is a positive gain and $V_i^*$ is the anisotropic Voronoi partition and assumed to be continuously updated.

**Proposition 2** *By applying the control law in (20), sensors in the physical space will converge asymptotically to a set of critical points i.e a set of anisotropic centroid Voronoi configurations. If this set is finite, the sensors converge to one of them.*

*Proof* The dynamics of sensors in the solution space (isotropic case) is given by

$$\dot{z}_i = \bar{u}_i, \tag{21}$$

From [1], it is well-known that the control input given by

$$\bar{u}_i = -k(z_i - C_{\bar{V}_i}) \tag{22}$$

drives sensors in the solution space to the centroidal Voronoi configuration, critical points of (11).

By using the chain rule, the control law in the physical space can be computed by

$$u = \dot{p}_i.$$
$$= \frac{\partial(\mathbf{F}^{-1} z_i)}{\partial z_i} \dot{z}_i.$$
$$= -k(p_i - C_{V_i^*}).$$

Consider $\mathscr{H}_{\mathscr{V}^*}$ as a Lyapunov function. Under the control law (20), $\frac{d}{dt} \mathscr{H}_{\mathscr{V}^*} \le 0$. By LaSalle's Principle, the sensors converge to the largest invariant set which is a set of anisotropic centroid Voronoi configurations. If this set consists of finite points, then the sensors converge to one of them (see Corollary 1.2 in [1]).

*Remark 2* This control law is distributed in the sense of Delaunay graph since each sensor only needs the current information of it's neighbor's position (but does not need to know how many neighbors it has) to compute the control as observable from (20). Moreover the algorithm could also

guarantee network connectivity since the Delaunay graph results in a connected graph (there is always a path connecting one sensor to the others). Taking out assumption 2 i.e. the case of fixed and unequal orientation will lead to the same control law. However in this case the control law will be non-distributed. Non-distributedness of an algorithm in multi-agent system is not prefered since the information that each agent has to process will increase with the increasing number of agents.

*Remark 3* Here, it is assumed that each sensor executes the algorithm synchronously with other sensors. However the algorithm can also be implemented in an asynchronous distributed fashion as shown in [1].

*Remark 4* The control law is optimal under the constraint of a fixed orientation. By considering the orientation as optimization variable (non-fixed orientation) as in the original problem will lead to a better result i.e. lower values of $\mathscr{H}$ are achieved.

A similar approach could also be applied to anisotropic sensors with arbitrary shapes for which a project matrix with similar properties as assumption 1 can be found. However some points have to be taken care. The first one is the question of what kind of Voronoi partition will be resulted from the chosen distance metric. Moreover the properties of the resulted Voronoi partiton have to be carefully investigated (e.g. can the Voronoi partition constructed in a distributed manner, etc). Another important issue that has to be paid attention is if the chosen distance metric represents the sensor model in the real world. For the analysis it may not be easily done in a straightforward manner since as shown in this paper, that the problem became difficult to deal with.

### 4.2 Collision avoidance guaranty

Another advantage of Voronoi approach is the implicit collision avoidance.

**Proposition 3** *With the control law (20), if there is no collision at $t^*$, there will be no collision at $t > t^*$.*

*Proof* Sensors applying the control law (20) will move towards centroid of its Voronoi cell as shown in Figure 5. From Lemma 2 and the continuity of $\phi(\cdot)$, the centroid is always inside the Voronoi cell and since the Voronoi tessellations are nonoverlapping by construction, no two sensors will come to the same point i.e there will be no collision between sensors for all $t \geq t^*$ if there was no collision at time $t^*$.
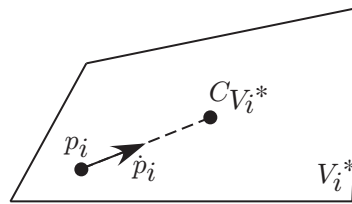


**Fig. 5** By the proposed control law, each sensor moves towards its centroid.

## 5 Numerical simulations

### 5.1 Convergence with Anisotropic sensors

First we illustrate the results above through simulation. Assume that there are 4 mobile sensors which sensor parameters $a, b, c, \theta$ are equal to $3, 1, 1, -\pi/2$, respectively. Region of interest $Q$ is a rectangle of $5 \times 4$ unit length. Density function $\phi(q) = 1, \forall q \in Q$. The initial position of mobile sensors are in the left-bottom side of region $Q$. Moreover, assume that at the initial time, $p_i \neq p_j, \forall i \neq j$ where $p_i = (x_i, y_i)$ i.e no collision occurs.

Each agent applies the control law (20). First each agent computes its own Voronoi partition and then computes its centroid. By the proposed control law, each sensor moves towards its centroid. Since the Voronoi partition depends on the agents' (and its neighbors) position, as soon as the sensor (or its neighbors) moves, a new Voronoi partition will be reconstructed (i.e. the Voronoi partition is continuously updated) and the sensor changes its direction to the centroid of the updated Voronoi partition. These steps are repeated until the agents converge to the final configuration. The results of applying the control law (20) are shown in Figure 6 where mobile sensors are deploying to cover the region of interest $Q$. Figures 6(a) and 6(b) show trajectories of sensors in the transformed and the real physical space respectively. The distance between the sensors during the deployment is shown in Figure 7. It can be observed that no collision occurs i.e. the distance between any two agents is larger than zero. Moreover, the decreasing of objective function can be observed from Figure 8. As shown in Figure 6(b), the mobile sensors converge to an anisotropic Voronoi configuration for a given sensor's orientation. For comparison, We conducted also a simulation for sensors with isotropic sensor model by considering a similar setup. The final configuration of sensors with isotropic sensor model is depicted in Figure 6(c). As depicted from Figures 6(b) and 6(c), note that both anisotropic and isotropic sensor models converge to a different configuration.
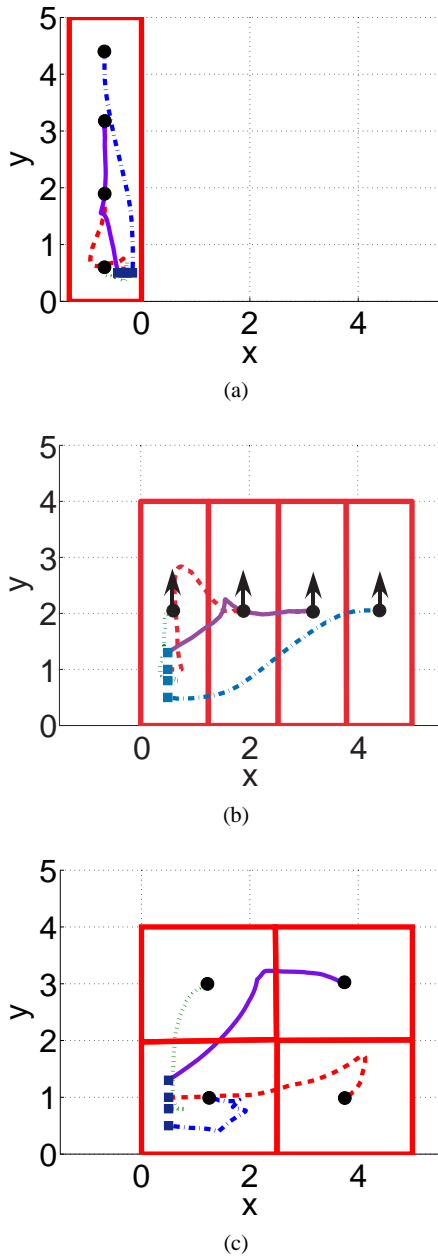
(a)



(b)



(c)

**Fig. 6** Trajectories of the sensors in (a) solution space, (b) real physical space. The square and circle signs show the initial and final position of the agents respectively, (c) the trajectories of the mobile sensors with isotropic sensor model. The anisotropic and isotropic Voronoi partition in (b) and (c) are constructed from the final position i.e. they are the dominance region of each sensor in the final configuration.

## 5.2 Number of agents vs. convergence speed

Next, the influence of the number of agents to the convergence speed of the system is studied. For the simulation setting, the parameters of the anisotropic sensors $a, b, c, \theta$ are equal to $2, 1, 1, -\pi/6$, respectively. The region $Q$ is a square region of side length $l = 10$ unit length with $\phi(q) = 1$, $\forall q$. The number of agents are varied from 5 to 60 agents. Initial
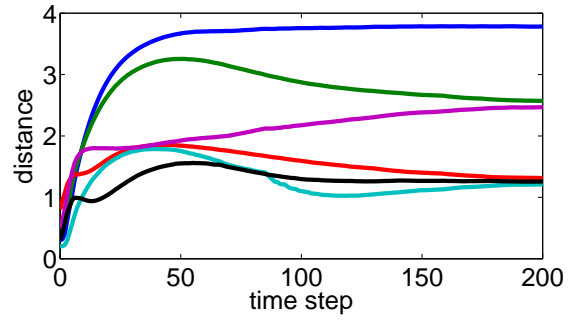


**Fig. 7** The distance between the anisotropic sensors. As shown, the distance is larger than zero i.e. no collision occurs.
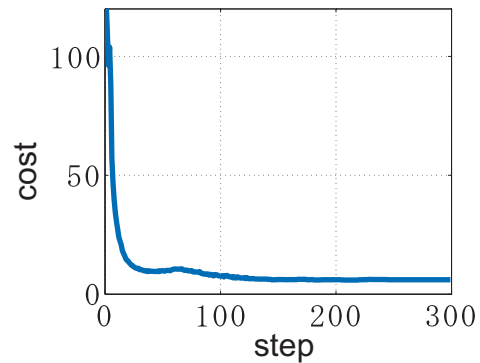


**Fig. 8** Cost (objective function) for anisotropic sensor in the real space.

position are chosen randomly from a square region of side length 3.5 unit length in the middle of the region $Q$ for the different agent numbers as shown in Figure 9. The settling time is used as a metric of the convergence speed which is defined as the number of steps needed to achieve a value in a range of 10% of the final cost. The simulation result of anisotropic sensor model for different number of agents is shown in Figure 10. It has been shown analytically that in the one-dimensional case, the convergence rate of Lloyd algorithm slows down as the number of generators becomes large [15]. Here numerical analysis indicates a similar result for the two-dimensional case and the anisotropic sensor model, i.e. large number of agents leads to a slower convergence speed (the settling time is larger). On the other hand, utilizing a large number of agents will lead to a lower final cost as shown in Figure 11. Hence there exists a trade-off between the final cost and convergence speed (settling time) w.r.t the number of agents in the system. Moreover, it will result in a higher robustness to agents/sensors failures since for a large number of agents, the final cost is not significantly different (Figure 11). Note however that, large number of sensors are expensive in terms of the sensors cost.
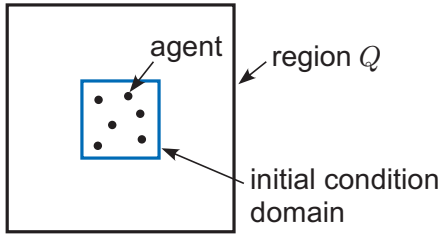
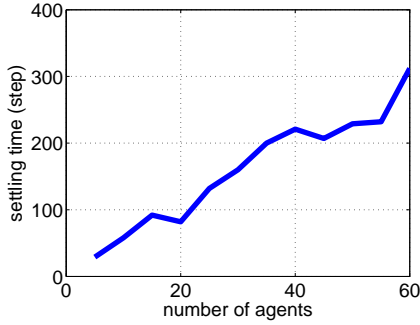**Fig. 9** Example of initial condition for numerical analysis.



**Fig. 10** Number of agents vs. settling time for anisotropic sensor model. Increasing number of agents slows down the convergence speed.
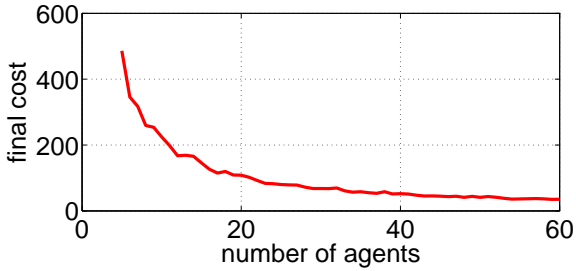


**Fig. 11** Number of agents vs. final cost for anisotropic sensor.

# 6 Experiments

In order to validate the theoretical results, experiments were conducted on a robotic testbed.

## 6.1 Experimental setup

In this experiment, we use three wheeled inverted pendulum embedded robots (Figure 12). A MTV-7310 camera mounted above the robots with a resolution of $470 \times 570$ is used to detect robot positions and orientations. The video signals are available in real time via a frame grabber board PicPort-Stereo-HrD and image processing software HALCON. The sampling period of the controller and the frame rate provided by the camera are 0.33[ms] and 30 [fps], respectively. The position and orientation of the robots are calculated by using the image processing. Based on these information,
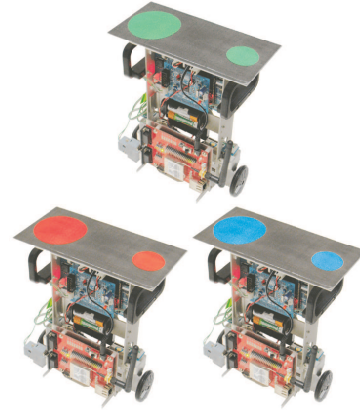


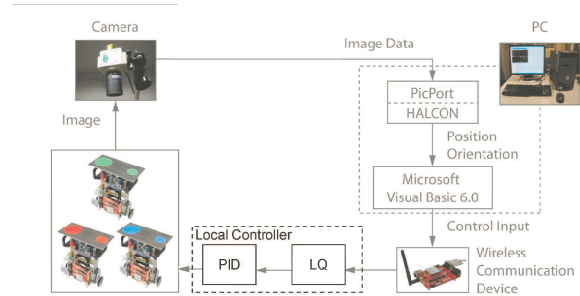**Fig. 12** Two-wheeled inverted pendulum robot.



**Fig. 13** Information flow chart.

the PC computes the velocity control input and sends it to each robot via the embedded wireless communication device Wiport (LANTRONIX). The Wiport attached to each robot recieves the signal and sends it to the microcomputer via serial communications. Stabilization of the inverted pendulum robot used in the experiment is achieved by an linear quadratic intergral optimal controller where the computed velocity control input is added to the desired value of this local controller. Figures 13 and 14 illustrate the information flow chart and the experimental environment including the robots, camera and PC, repectively.

The inverted pendulum robots motion can be approximately represented by

$$\dot{\theta}_i = \omega_i,$$
$$\dot{x}_i = v_i \cos \theta_i, \qquad (23)$$
$$\dot{y}_i = v_i \sin \theta_i,$$

where $(\omega_i, v_i)$ are control inputs for robot $i$.

## 6.2 Experiment 1: Convergence with anisotropic sensors

The first experiment discussed is the convergence of the control laws. For the experiment, the region of interest is a rect-
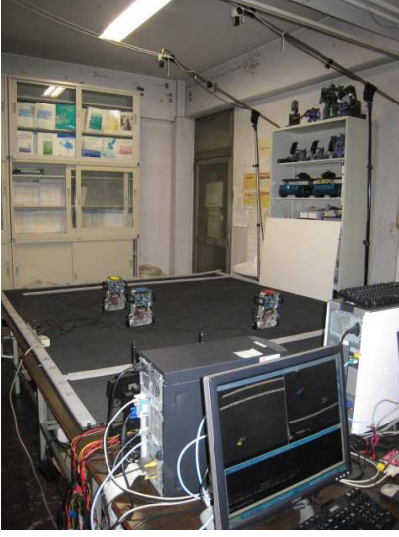
**Fig. 14** Experiment environment.



**Fig. 15** Results of experiment 1 (convergence with anisotropic sensors): robot trajectory in $X - Y$ plane. The $\bigcirc, \square$ signs show the initial and final posisiton of the robots respectively.

angle with uniform density function $\phi(q) = 1, \forall q \in Q$. Assume that the robots are equipped with anisotropic sensors which sensor parameters $a, b, c, \theta$ are equal to $2, 1, 1, 0$. For the dynamics given in (23), the control inputs (20) can be modified into ( [1])

$$\omega_i = 2k_\omega \arctan \frac{(-\sin\theta_i, \cos\theta_i) \cdot (p_i - C_{V_i^*})}{(\cos\theta_i, \sin\theta_i) \cdot (p_i - C_{V_i^*})}, \qquad (24)$$

$$v_i = -k_v(\cos\theta_i, \sin\theta_i) \cdot (p_i - C_{V_i^*}), \qquad (25)$$

where $p_i$ and $C_{V^*}$ are agent $i$-th current position and centroid of anisotropic Voronoi partition respectively. In the experiment, we set the gains $k_v, k_\omega$ to 0.006 and 0.5 respectively.

The results of experiment 1 are shown in Figure 15. Theoretically, the control law shows convergent property. However, in order for the two-wheeled inverted pendulum robot to maintain its stability, we define that an agent converges to the centroid of its anisotropic Voronoi partition when the agent is within a certain threshold of the target position. As indicated in Figure 15, the robots converge within a certain threshold to the anisotropic Voronoi configuration.

### 6.3 Experiment 2: Robustness to sensor failure

In experiment 2, we investigate robustness of our algorithm in the presence of failure agent. We assume that after the robots converged to an anisotropic Voronoi configuration, one robot which is the robot at the bottom of Figure 15 fails. Moreover, we assume that the other robots can detect which agent fails. As shown in Figure 16, the robots left re-deploy themselves until they converge to a new anisotropic Voronoi configuration. Thus, the experiment results validate the robustness of the control laws.
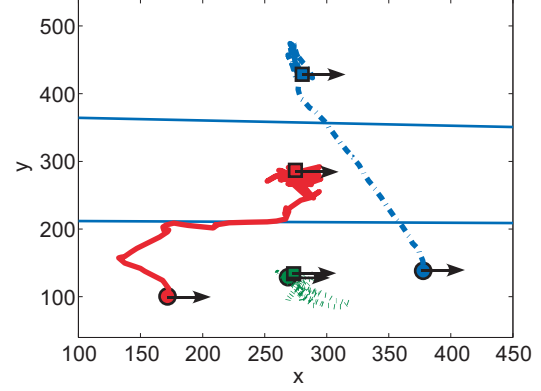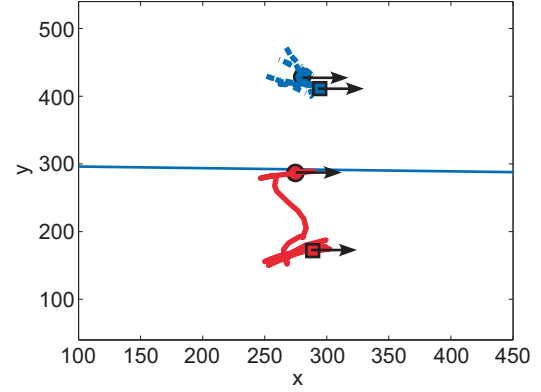


**Fig. 16** Results of experiment 2 (robustness to sensor failure): trajectory of the robots in $X - Y$ plane. The $\bigcirc, \square$ signs show the initial and final posisiton of the robots respectively.

### 6.4 Towards implementation on real robotic systems

The effectiveness of the proposed algorithm has been shown through small scale experimental setup. In order to move from experimental evaluation to the implementation on real robotic systems, some (hardware) requirements have to be fulfilled. The main hardware requirements are localization technology, communication networks and sensors. The localization technology is required to get the position information of the sensors. In the experiment, we used bird-eye camera to get the location of each robot. In real robot systems, GPS technology could be one solution to solve the localization problem. Another important tool is communication networks. Each robot needs to be equipped with a communication network so that it can communicate with each other e.g. sending information of its position and orientation. In our experiment, the robot did not exchange information directly but rather to get the information from a

centralized computer. In real robot systems, each robot can be equipped with wireless communication technology (e.g. Zig-bee, Wi-Fi) to directly communicate (exchange information) with each other. Moreover, each robot also has to be equipped with on board computation so that the robot could decide/compute its next action by its own. By satisfying these requirements, the algorithm could be implemented in a real world scenario.

## 7 Conclusion and future works

In this paper a first approach for the coverage control with an anisotropic sensor model is presented. The anisotropic sensors considered in this paper are assumed to have elliptic sensing performance level sets. An optimal control law for fixed and equal orientation is derived using a Voronoi based approach with an adapted Lloyd algorithm and a gradient descent approach. The control law is distributed and also guarantees collision avoidance. The efficacy of the proposed control law is confirmed by simulation and experiments. Currently, the problem with the orientation as optimization variable and a method to make the related control law distributed (some relevant problem as in [14]) are investigated. Future work addresses the use of more general anisotropic sensor models and a more suitable alternative approach.

## References

1. J. Cortes, S. Martinez, T. Karatas, F. Bullo, "Coverage control for mobile sensing networks," *IEEE Transactions on Robotics and Automation*, Vol. 20, No. 2, pp. 243-255, 2004.
2. J. Cortes, S. Martinez, F. Bullo, "Spatially-distributed coverage optimization and control with limited-range interactions," *ESAIM. Control, Optimisation & Calculus of Variations*, Vol. 11, pp. 691-719, 2005.
3. A. Kwok and S. Martinez, "Energy-balancing cooperative strategies for sensor deployment," *IEEE Conference on Decision and Control*, pp. 6136-6141, 2007.
4. W. Li and C. G. Cassandras, "Distributive cooperative coverage control of sensor networks," *IEEE Conference on Decision and Control*, pp. 2542-2547, 2005.
5. A. Howard, M. J. Mataric and G. S. Sukhatme, "Mobile sensor network deployment using potential fields : a distributed, scalable solution to the area coverage problem," *Proc. 6th Int. Symposium on Distributed Autonomous Robotics Systems*, pp. 299-308, 2002.
6. D. V. Dimarogonas and K. J. Kyriakopoulos, "An inverse agreement control strategy with application to swarm dispersion," *IEEE Conference on Decision and Control*, pp. 6148-6153, 2007.
7. I. I. Hussein and D. M. Stipanovic, "Effective coverage control for mobile sensor networks with guaranteed collision avoidance," *IEEE Transactions on Control Systems Technology*, Special Issue on Multi-Vehicle Systems Cooperative Control with Applications, Vol. 15, No. 4, pp. 642-657, 2007.
8. N. Hubel, S. Hirche, A. Gusrialdi, T. Hatanaka, M. Fujita and O. Sawodny, "Coverage control with information decay in dynamic environments," *17th IFAC World Congress*, pp. 4180-4185, 2008.
9. P. F. Hokayem, D. M. Stipanovic and M. W. Spong, "Dynamic coverage control with limited communication," *The American Control Conference*, pp. 4878-4883, 2007.
10. P. F. Hokayem, D. M. Stipanovic and M. W. Spong, "On persistent coverage control," *IEEE Conference on Decision and Control*, pp. 6130-6135, 2007.
11. L. Favalli, P. Gamba, T. Gatti and A. Mecocci, "Multi-radar data fushion for object tracking and shape estimation," *Signal Processing*, Vol. 48, No. 3, pp. 235-239, 1996.
12. F. Labelle and J. R. Shewchuk, "Anisotropic voronoi diagrams and guaranteed-quality anisotropic mesh generation," *Proceedings of the 19th ACM Symposium on Computational Geometry*, pp. 191-200, 2003.
13. Y. Igarashi, M. Fujita and M. W. Spong, "Passivity-based 3D Attitude Coordination: Convergence and Connectivity," *Proceedings of the IEEE Conference on Decision and Control*, pp. 2558-2565, 2007.
14. L. Feng, I. Hotz, B. Hamann and K. I. Joy, "Anisotropic noise samples," *IEEE Transactions on Visualization and computer graphics*, Vol. 14, No. 2, pp. 342-354, 2008.
15. Q. Du, M. Emelianenko and L. Ju, "Convergence of the Lloyd algorithm for computing centroidal Voronoi tessellations," *SIAM Journal on Numerical Analysis*, pp. 102-119, 2006